WeibPar

Time Dependent Theory Guide

Dynamic Fatigue Parameter Estimation

CONNECTICUT RESERVE TECHNOLOGIES, INC.

Introduction

Ceramic materials can easily exhibit complex thermomechanical behavior that is both inherently time-dependent and hereditary in the sense that current behavior depends not only on current conditions, but also on thermomechanical history. The ability of a brittle material component to sustain load degrades over time due to a variety of effects such as oxidation, creep, stress corrosion, and fatigue. The design methodology presented in this report combines the statistical nature of strength-controlling flaws with the mechanics of crack growth. Using the fast fracture and fatigue parameters, as well as the results obtained from a finite element analysis, component reliability as a function of time can be computed. The NASA CARES/Life algorithm embodies these concepts and this software was utilized in analyzing the model parameters and in determining component life. Life can be assessed in terms of time to failure, or in terms of cycles to failure. With this type of reliability algorithm, the gun barrel design engineer can make appropriate design changes until an acceptable component life has been computed. In addition to the fast fracture parameters, i.e, the Weibull shape and scale parameters, the analysis of time-dependent reliability necessitates evaluation of distinct parameters relating to fatigue crack growth and fatigue life. The theoretical development that supports the estimation of fatigue parameters is outlined in this report.

Under this task estimation methods for the geometry independent parameters needed for time dependent (sub-critical crack growth) component reliability analyses were established for data obtained using either the C-ring and the sectored flex bar. These geometry independent parameters (B_V and B_A) are similar to the material specific characteristic strengths (σ_{0V} and σ_{0A}) parameters needed to conduct a fast fracture component analysis. The NASA CARES/Life algorithm has estimation methods established for B_V and B_A that are associated with a limited number of specimen configurations, but these specimen configurations do not include the C-ring or the sectored flex bar. It was proposed that estimates for the power law exponent N, and the geometry independent parameter, B be extracted from the time dependent ceramic data generated by ARL. However, at the time this report was prepared the requisite time dependent failure data was not available. Establishing confidence bounds on the time dependent material parameters using bootstrap techniques is briefly discussed along with the feasibility of incorporating the requisite computational methods into a parameter estimation computer algorithm. Finally, since a limited amount of time dependent ceramic failure data will be made available early in the project, an effort to explore and establish pooling procedures for time dependent parameter estimation will be conducted.

Subcritical Crack Growth

Ceramics exhibit the phenomenon of delayed fracture or fatigue. With load histories at stress levels that do not induce fast fracture, there is a regime where subcritical crack growth (SCG) occurs. Subcritical crack growth involves a combination of simultaneous, deleterious and synergistic failure mechanisms. These can be grouped into two categories: (1) crack growth due to stress corrosion, and (2) crack growth due to mechanical effects arising from cyclic loading. Stress corrosion reflects a stress-dependent chemical interaction between the material and its

environment. Water, for example, has a pronounced deleterious effect on the strength of ceramics. Higher temperatures also tend to accelerate this process.

Models for SCG that have been developed tend to be semi-empirical and approximate the behavior of crack growth phenomenologically. Experimental data indicates that crack growth rate is a function of the applied stress intensity factor (or the range in the stress intensity factor). Curves of experimental data show three distinct regimes or regions of growth when the data is graphically depicted as the logarithm of the rate of crack growth versus the logarithm of the mode I stress intensity factor (reference Figure 1). The first region indicates threshold behavior of the crack, where below a certain value of stress intensity the crack growth is zero. The second region shows an approximately linear relationship of stable crack growth. The third region indicates unstable crack growth as the materials critical stress intensity factor is approached.

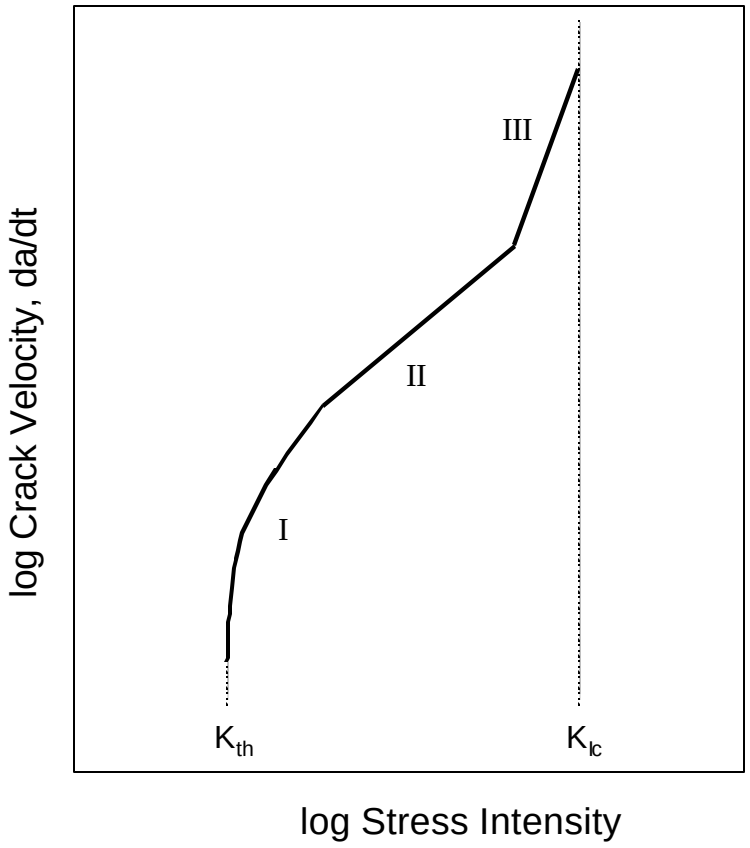

Figure 1 Crack Velocity as a Function of Stress Intensity (*K)* in Monolithic Ceramics. Crack Initation Does Not Occur when $K<K_{th}$. SCG can occur when $K_{th}<K<K_{Ic}$. Fracture occurs when $K> K_{Ic}$. (Regions I, II, and III)

The second region typically dominates the life of the material. For the stress corrosion failure mechanism, these curves are material and environment sensitive. The most often cited models in the literature regarding SCG are based on power law formulations for the rate equations. Power law formulations are used to model the second region of the experimental data cited above for both the stress corrosion and the fatigue. This power law formulation is expressed as

$$\begin{aligned} \frac{da(x,y,z,t)}{dt} &= A\, K_{Ieq}^{N}(x,y,z,t) \\ &= A\, s_{Ieq}{}^{N}(x,y,z,t)\, Y^{N}\, a(x,y,z,t) \end{aligned} \qquad \textbf{(1)}$$

where A and N (crack growth exponent) are material/environmental constants and $s_{Ieq}(x,y,z,t)$ is the mode I stress. In order to utilize this relationship in a reliability setting, the mode I stress $s_{Ieq}(x,y,z,t_f)$ at the time of failure ($t = t_f$) is transformed to its critical effective stress distribution at time $t = 0$. The transformation is obtained by solving the following classical fracture mechanics expression for the crack length a

$$K_{Ieq}(x,y,z,t) = s_{Ieq}(x,y,z,t)\, Y \sqrt{a(x,y,z,t)} \qquad \textbf{(2)}$$

where Y is a function of crack geometry, and $a(x,y,z,t)$ represents the crack length at time t. Differentiating the resulting expression for a with respect to time, and setting this differential equation equal to the right hand side of equation 1 yields the following expression

$$s_{Ieq,0}(x,y,z,t_f) = \left[\frac{\int_0^{t_f} s_{Ieq}^{N}(x,y,z,t)\, dt}{B} + s_{Ieq}^{N-2}(x,y,z,t_f) \right]^{\frac{1}{(N-2)}} \qquad \textbf{(3)}$$

where

$$B = \frac{2}{A\, Y^{2}\, K_{IC}^{N-2}\, (N-2)} \qquad \textbf{(4)}$$

is a material/environmental fatigue parameter, K_{Ic} is the critical stress intensity factor, and $s_{Ieq}(x,y,z,t_f)$ is the equivalent stress distribution in the component at time $t = t_f$. The parameter B has units of $stress^2 \times time$. Note that Y is assumed constant for subcritical crack growth. The parameter A, Y and K_{Ic} are never computed directly, but are manifested through the parameter B via the expression above when a value for the parameter B is estimated from experimental data. The transformation given by equation 3 permits the use of the Weibull fast fracture expressions in evaluating time dependent component reliability. The use of equation 4 strongly implies that the parameter B is inherently tied to a specific defect population through the use of Y and K_{Ic}.

The subcritical crack growth model is combined with a two-parameter Weibull cumulative distribution function to characterize the component failure probability as a function of service lifetime. This is accomplished by equating s_e with $s_{Ieq,0}$. Multiaxial stress fields are included by

using the principle of independent action (PIA) model, or the Batdorf theory. These multiaxial reliability expressions were outlined in the previous discussion on time-independent reliability analysis models.

SCG Model for Creep (Static Fatigue) – Tensile Specimen

Creep loading, also known as static fatigue to the ceramist, is defined by the engineer as the application of a constant load over time. To the ceramist creep defines a specific type of deformation mechanism. This report adopts the engineer's viewpoint as well as the engineering nomenclature for describing time dependent load histories in general. For this load case the mode I equivalent stress, $s_{Ieq}(x,y,z,t)$, is independent of time and is thus denoted by $s_{Ieq}(x,y,z)$. Integrating the right hand side of equation 3 with respect to time yields

$$s_{Ieq,0}(x,y,z,t_f) = s_{Ieq}(x,y,z)\left[\frac{t_f\, s_{Ieq}^{2}(x,y,z)}{B} + 1\right]^{\frac{1}{N-2}} \quad \textbf{(5)}$$

SCG Model for Monotonic Load (Dynamic Fatigue) – Tensile Specimen

Monotonically increasing uniaxial loading, also know as dynamic fatigue to the ceramist, is defined as the application of a constant stress rate $\dot{s}\ (x, y, z)$ over a period of time, t. Assuming the applied stress is zero at time $t=0$, then

$$s_{Ieq}(x,y,z,t) = t\left(\frac{ds(x,y,z)}{dt}\right) \quad \textbf{(6)}$$

Substituting equation 6 into equation 3 results in the following expression for effective stress

$$s_{Ieq,0}(x,y,z) = \left[\frac{s_{Ieq}^{N}(x,y,z,t=t_f)\ t_f}{(N+1)B} + s_{Ieq}^{N-2}(x,y,z,t=t_f)\right]^{\frac{1}{N-2}} \quad \textbf{(7)}$$

Parameter Estimation – Tensile Dynamic Fatigue Data

The approach for computing the time dependent strength parameters B and N from failure data is presented in this section for a specific specimen geometry, i.e., a uniaxial test specimen. Hence the stress state is uniform throughout the specimen, and is not spatially dependent. This is not the case for C-ring specimens, or sectored flex bars (see next section) that will be used to characterize material properties in this program. Begin by expressing the uniaxial formulation of the probability of failure as

$$\begin{aligned} P_f &= 1 - \exp\left[-\left(\frac{1}{s_{0V}} \right)^{m_V} \int_V \left[s_{Ieq,0}\left(x,y,z,t_f\right) \right]^{m_V} dV \right] \\ &= 1 - \exp\left[-\left(\frac{\tilde{s}\left(t_f\right)}{s_{0V}} \right)^{m_V} \int_V dV \right] \end{aligned} \tag{8}$$

for flaw distributions distributed through the volume of all test specimens (a similar expression exists for surface flaw distributions). Here $\tilde{s}$ is referred to the inert strength in the ceramics literature (e.g., Appendix in ASTM C 1368). Under the assumption that

$$\left(\frac{\hat{s}}{\tilde{s}} \right)^{N-2} << 1 \tag{9}$$

where $\hat{s}$ is the stress at failure. For monotonically increasing stress tests (dynamic fatigue) equation 7 simplifies to

$$\begin{aligned} \tilde{s}\left(t_f\right) &= \left[\frac{\left(\hat{s}\right)^N t_f}{\left(N+1\right) B} \right]^{\frac{1}{N-2}} \\ &= \left[\frac{\left(\hat{s}\right)^{N+1}}{\left(N+1\right) B \dot{\hat{s}}} \right]^{\frac{1}{N-2}} \end{aligned} \tag{10}$$

under the assumption indicated in equation 9. Thus the stress at failure $\hat{s}$ can be expressed as

$$\left(\hat{s}\right)^{N+1} = \left(N+1\right) B \left(\tilde{s}\right)^{N-2} \dot{\hat{s}} \tag{11}$$

Now let

$$\left(D\right)^{N+1} = \left(N+1\right) B \left(\tilde{s}\right)^{N-2} \tag{12}$$

then

$$\left(\hat{s}\right)^{N+1} = \left(D\right)^{N+1} \dot{\hat{s}} \tag{13}$$

Taking the natural log of both sides of equation 13 yields

$$\ln(\hat{s}) = \ln(D) + \left(\frac{1}{N+1}\right)\ln(\dot{\hat{s}}) \quad \textbf{(14)}$$

Thus plotting the log of the stress at failure $\hat{s}$ against the log of the applied stress rate $\dot{\hat{s}}$ should yield a straight line with a slope of *[1/(N+1)]*. Typically linear regression techniques are used to determine the parameters *N* and *D*. Once these parameters are determined from the time dependent failure data this information would be combined with the Weibull distribution parameter estimates and the parameter *B* would be computed from the expressions developed below.

Substitution of equation 10 into equation 8 yields

$$\begin{aligned} P_f &= 1 - \exp\left[-\left(\frac{1}{s_{0V}}\right)^{m_V} \left[\frac{(\hat{s})^{N+1}}{(N+1)B\,\dot{\hat{s}}}\right]^{\frac{m_V}{N-2}} \int_V dV \right] \\ &= 1 - \exp\left[-\left(\frac{1}{s_{0V}}\right)^{m_V} \left[\frac{(\hat{s})^{N+1}}{(N+1)B\,\dot{\hat{s}}}\right]^{\frac{m_V}{N-2}} V_{gage} \right] \end{aligned} \quad \textbf{(15)}$$

Solving this expression for $\hat{s}$ yields

$$(\hat{s})^{N+1} = \left\{\left(\frac{1}{V_{gage}}\right)\ln\left[\frac{1}{1-P_f}\right]\right\}^{\frac{N-2}{m_V}} (s_{0V})^{N-2}(N+1)B\,\dot{\hat{s}} \quad \textbf{(16)}$$

Comparing equation 11 and 16 leads to

$$(D)^{N+1} = \left\{\left(\frac{1}{V_{gage}}\right)\ln\left[\frac{1}{1-P_f}\right]\right\}^{\frac{N-2}{m_V}} (s_{0V})^{N-2}(N+1)B \quad \textbf{(17)}$$

and solving for B from this last expression yields

$$B = \frac{(D)^{N+1}}{\left\{\left(\frac{1}{V_{gage}}\right)\ln\left[\frac{1}{1-P_f}\right]\right\}^{\frac{N-2}{m_V}} (s_{0V})^{N-2}(N+1)} \quad \textbf{(18)}$$

In order to compute the parameter *B* from equation 18 a probability of failure must be utilized. The simplest approach would be to take

$$P_f = .50 \tag{19}$$

since linear regression methods are used. Also note that the parameter N will be independent of the specimen geometry used to generate time to failure data, whereas the parameter D is strongly dependent on the specimen geometry. This is similar to the fast fracture Weibull parameters, i.e., m is not dependent on the specimen geometry where s_q is. Noting that D is specimen dependent, keep in mind that the development above was presented for creep in a uniaxial test specimen. The next section develops an expression for B for generic test specimens.

Parameter Estimation – Dynamic Fatigue Data, Arbitrary Specimen Geometry

The approach for computing the time dependent strength parameters B and N from failure data for an arbitrary specimen geometry is presented in this section. Here the stress state and stressing rate are assumed to vary spatially throughout the specimen. Begin by expressing the probability of failure as

$$\begin{aligned} P_f &= 1 - \exp\left[-\left(\frac{1}{s_{0V}}\right)^{m_V} \int_V \left[s_{Ieq,0}\left(x,y,z,t_f\right)\right]^{m_V} dV \right] \\ &= 1 - \exp\left\{ -\left(\frac{1}{s_{0V}}\right)^{m_V} \int_V \left[\tilde{s}\left(t_f\right)\right]^{m_V} dV \right\} \end{aligned} \tag{20}$$

This uniaxial stress formulation will be expanded to include multiaxial stress states momentarily. The uniaxial formulation here is strictly for convenience. Noting that

$$\hat{s} = \hat{s}\left(x,y,z\right) \tag{21}$$

and the stressing rate are spatially dependent, but

$$t_f = \frac{\hat{s}}{\dot{\hat{s}}} \tag{22}$$

is constant throughout the specimen geometry, i.e., t_f is not spatially dependent. Inserting the results from equations 10 and 22 into equation 20 yields

$$P_f = 1 - \exp\left\{-\left(\frac{1}{s_{0V}}\right)^{m_V}\left[\frac{1}{(N+1)B}\right]^{\frac{m_V}{N-2}}\int_V\left[\frac{(\hat{s})^{N+1}}{\dot{\hat{s}}}\right]^{\frac{m_V}{N-2}}dV\right\}$$
$$= 1 - \exp\left[-\left(\frac{1}{s_{0V}}\right)^{m_V}\left[\frac{t_f}{(N+1)B}\right]^{\frac{m_V}{N-2}}\int_V(\hat{s})^{\frac{Nm_V}{N-2}}dV\right] \quad \textbf{(23)}$$

If we identify

$$m_1 = \frac{m_V}{N-2} \quad \textbf{(24)}$$

and

$$m_2 = \frac{N\,m_V}{N-2} \quad \textbf{(25)}$$

then

$$P_f = 1 - \exp\left[-\left(\frac{1}{s_{0V}}\right)^{m_V}\left[\frac{t_f}{(N+1)B}\right]^{m_1}\int_V(\hat{s})^{m_2}dV\right] \quad \textbf{(26)}$$

Next, identify $s_{\max}$ as the maximum stress in the arbitrary component associated with the failure stress distribution $\hat{s} = \hat{s}(x, y, z)$, then

$$P_f = 1 - \exp\left[-\left(\frac{1}{s_{0V}}\right)^{m_V}\left[\frac{t_f}{(N+1)B}\right]^{m_1}(s_{\max})^{m_2}\int_V\left(\frac{\hat{s}}{s_{\max}}\right)^{m_2}dV\right] \quad \textbf{(27)}$$

In the Task #1 Report entitled "*Evaluation of Effective Volume & Effective Area for C – Ring Test Specimen"* prepared under the previous contract the integral appearing in equation 27 was identified as an effective volume, i.e.,

$$kV_T = \int_V\left(\frac{s}{s_{\max}}\right)^{m_2}dV \quad \textbf{(28)}$$

Here the subscript T emphasizes that this effective volume is a "temporal" effective volume. The modulus m_2 is not the fast fracture Weibull modulus as it was in the previous report. This modulus is a function of the fast fracture modulus and the power law exponent, as indicated in equation 25.

Now equation 27 can be written as

$$P_f = 1 - \exp\left[-\left(\frac{1}{s_{0V}}\right)^{m_V} \left[\frac{t_f}{(N+1)B}\right]^{m_1} (s_{\max})^{m_2} kV_T \right] \quad \textbf{(29)}$$

and with

$$t_f = \frac{\hat{s}(x,y,z)}{\dot{\hat{s}}(x,y,z)} = \frac{\hat{s}_{\max}}{\dot{\hat{s}}_{\max}} \quad \textbf{(30)}$$

then

$$P_f = 1 - \exp\left\{ -\left(\frac{1}{s_{0V}}\right)^{m_V} \left[\frac{1}{(N+1)B}\right]^{m_1} \left[\frac{(\hat{s}_{\max})^{N+1}}{\dot{\hat{s}}_{\max}}\right]^{m_1} kV_T \right\} \quad \textbf{(31)}$$

From equation 13, one can deduce that

$$(D)^{N+1} = \frac{(\hat{s}_{\max})^{N+1}}{\dot{\hat{s}}_{\max}} \quad \textbf{(32)}$$

which further simplifies equation 31, i.e.,

$$P_f = 1 - \exp\left\{ -\left(\frac{1}{s_{0V}}\right)^{m_V} \left[\frac{(D)^{N+1}}{(N+1)B}\right]^{m_1} kV_T \right\} \quad \textbf{(33)}$$

Noting that this derivation has focused on strength limiting flaws distributed through the volume, at this point the notation B_V, N_V and D_V are adopted. This infers that these time dependent parameters are associated with a volume flaw population. Hence this last expression can be solved for the parameter B_V such that

$$B_V = \frac{(D_V)^{N_V+1}}{\left\{\left(\frac{1}{kV_T}\right)\ln\left[\frac{1}{1-P_f}\right]\right\}^{\frac{N_V-2}{m_V}} (s_{0V})^{N_V-2}(N_V+1)} \quad \textbf{(34)}$$

A similar derivation for strength limiting flaws distributed along the surface of test specimens would lead to the following expression

$$B_A = \frac{(D_A)^{N_A+1}}{\left\{\left(\frac{1}{kA_T}\right)\ln\left[\frac{1}{1-P_f}\right]\right\}^{\frac{N_A-2}{m_V}} (s_{0V})^{N_A-2}(N_A+1)} \quad \textbf{(35)}$$

where kA_T is the "temporal" effective area for the specimen being analyzed.

Data Analysis

At the time this report was written time dependent data provided by ARL was not available for any of the candidate ceramics under consideration as gun barrel material. In order to demonstrate how the approach outlined above can be implemented, a silicon nitride data base (NT551 - Saint Gobain/Norton Industrial Ceramics) available in the open literature (Andrews et al., 1999) was utilized. Data tables associated with the Saint Gobain material are included in this report to help clarify the procedure, and this information is referred to as the "Andrews data." This failure data includes several temperatures, stressing rates and specimen geometries. However, this report focused on the room temperature bend bar data (ASTM 1161 – B specimen geometry) in order to assure the data under consideration was attributable to the sub-critical crack growth failure mechanism, and not a creep failure mechanism which can occur at elevated temperatures.

Three stressing rates are available at room temperature in the Andrews data. Fast fracture Weibull parameters were estimated from the highest stressing rate data (30 MPa/sec – see Table I). The Andrews data provided at the highest stressing rate were associated with surface defects. However, this data was censored due to the presence of exclusive flaws. Eight failure strengths from the highest stressing rate data were identified as belonging to an "exclusive flaw population." The fast fracture parameter estimation techniques available in ASTM C 1239 are only applicable to "concurrent flaw populations." Thus these eight pieces of information were not used in the calculations of the Weibull parameters. From this censored information an unbiased Weibull modulus of $m_A = 8.98$ and a characteristic strength of $(s_q)_A = 805.86\ MPa$ were established. Based on the B-specimen bend bar geometry tested under specifications set forth in ASTM 1161, the material specific strength was established at $(s_0)_A = 1{,}337.4\ MPa \cdot (mm)^{0.111}$. As indicated in the discussions in the previous section, the fast fracture Weibull parameters must be computed prior to establishing values for the time dependent parameters.

Next, the time dependent parameters N_A and D_A were computed employing linear regression techniques, and utilizing the data listed in Tables I through III. Note carefully that the data in all three tables have been censored. Two bend bar specimens from the intermediate stressing rate data (0.3 MPa/second) and five bend bar specimens from the low stressing rate data (0.003 MPa/second) failed from volume defects. A sixth bend bar specimen from the low stressing rate data failed outside the gage section. These data were censored in a very simple minded fashion, i.e., they were removed from the database prior to computing N_A and D_A. This

may not be rigorous, but currently censoring techniques for time dependent parameters have not been developed. If subcritical crack growth is a dominant failure mode, then issues such as censoring time dependent data should be addressed later in the project. Given the data in Tables I through III, then $N_A = 76$ and $D_A = 713.77$, where the units for D_A are consistent with *MPa* for stress, and *mm* for units of length.

Failure strength as a function of stressing rate for the data listed in Tables I through III, as well as the regression line based on the estimated values of N_A and D_A listed above are plotted in Figure 2.

Table I NT551 Fast Fracture Data from Andrews et al. (1999)

Test Temperature (°C)	Stress Rate MPa/s	Machining Direction (Transverse or Longitudinal)	Strength (MPa)	Flaw Type
20	30	Trans	705.47	SURFACE
20	30	Trans	707.23	SURFACE
20	30	Trans	710.60	SURFACE
20	30	Trans	751.86	SURFACE
20	30	Trans	773.06	SURFACE
20	30	Trans	777.69	SURFACE
20	30	Trans	778.47	SURFACE
20	30	Trans	779.89	SURFACE
20	30	Trans	792.33	SURFACE
20	30	Trans	793.37	SURFACE
20	30	Trans	796.46	SURFACE
20	30	Trans	804.46	SURFACE
20	30	Trans	820.27	SURFACE
20	30	Trans	832.23	SURFACE
20	30	Trans	832.43	SURFACE
20	30	Trans	834.38	SURFACE
20	30	Trans	869.07	SURFACE
20	30	Trans	869.13	SURFACE
20	30	Trans	870.81	SURFACE
20	30	Trans	888.87	SURFACE
20	30	Trans	922.28	SURFACE
20	30	Trans	926.12	SURFACE

Table II NT551 Failure Data at the Intermediate Stressing Rate, from Andrews et al. (1999)

Test Temperature (°C)	Stress Rate MPa/s	Machining Direction (Transverse or Longitudinal)	Strength (MPa)	Flaw Type
20	0.3	Trans	435.31	SURFACE
20	0.3	Trans	530.39	SURFACE
20	0.3	Trans	582.25	SURFACE
20	0.3	Trans	612.05	SURFACE
20	0.3	Trans	634.66	SURFACE
20	0.3	Trans	639.45	SURFACE
20	0.3	Trans	639.71	SURFACE
20	0.3	Trans	641.32	SURFACE
20	0.3	Trans	643.34	SURFACE
20	0.3	Trans	653.88	SURFACE
20	0.3	Trans	663.45	SURFACE
20	0.3	Trans	667.56	SURFACE
20	0.3	Trans	670.92	SURFACE
20	0.3	Trans	678.17	SURFACE
20	0.3	Trans	684.66	SURFACE
20	0.3	Trans	686.40	SURFACE
20	0.3	Trans	687.46	SURFACE
20	0.3	Trans	690.67	SURFACE
20	0.3	Trans	694.79	SURFACE
20	0.3	Trans	701.64	SURFACE
20	0.3	Trans	701.66	SURFACE
20	0.3	Trans	713.92	SURFACE
20	0.3	Trans	717.68	SURFACE
20	0.3	Trans	726.28	SURFACE
20	0.3	Trans	735.74	SURFACE
20	0.3	Trans	739.71	SURFACE
20	0.3	Trans	740.71	SURFACE
20	0.3	Trans	744.72	SURFACE
20	0.3	Trans	788.99	SURFACE
20	0.3	Trans	825.48	SURFACE

Table III NT551 Failure Data at the Lowest Stressing Rate, from Andrews et al. (1999)

Test Temperature (°C)	Stress Rate MPa/s	Machining Direction (Transverse or Longitudinal)	Strength (MPa)	Flaw Type
20	0.003	Trans	517.67	SUR-MD
20	0.003	Trans	517.43	SUR-MD
20	0.003	Trans	584.76	SUR-MD
20	0.003	Trans	596.40	SUR-MD
20	0.003	Trans	611.07	SUR-MD
20	0.003	Trans	622.29	SUR-MD
20	0.003	Trans	556.71	SUR-MD
20	0.003	Trans	557.77	SUR-MD
20	0.003	Trans	577.89	SUR-MD
20	0.003	Trans	606.03	SUR-MD
20	0.003	Trans	571.32	SUR-MD
20	0.003	Trans	642.15	SUR-MD
20	0.003	Trans	606.28	SUR-MD
20	0.003	Trans	588.29	SUR-MD
20	0.003	Trans	588.55	SUR-MD
20	0.003	Trans	609.60	SUR-MD
20	0.003	Trans	600.08	SUR-MD
20	0.003	Trans	645.94	SUR-MD
20	0.003	Trans	620.49	SUR-MD
20	0.003	Trans	627.12	SUR-MD
20	0.003	Trans	634.75	SUR-MD
20	0.003	Trans	641.24	SUR-MD
20	0.003	Trans	651.31	SUR-MD
20	0.003	Trans	676.77	SUR-MD

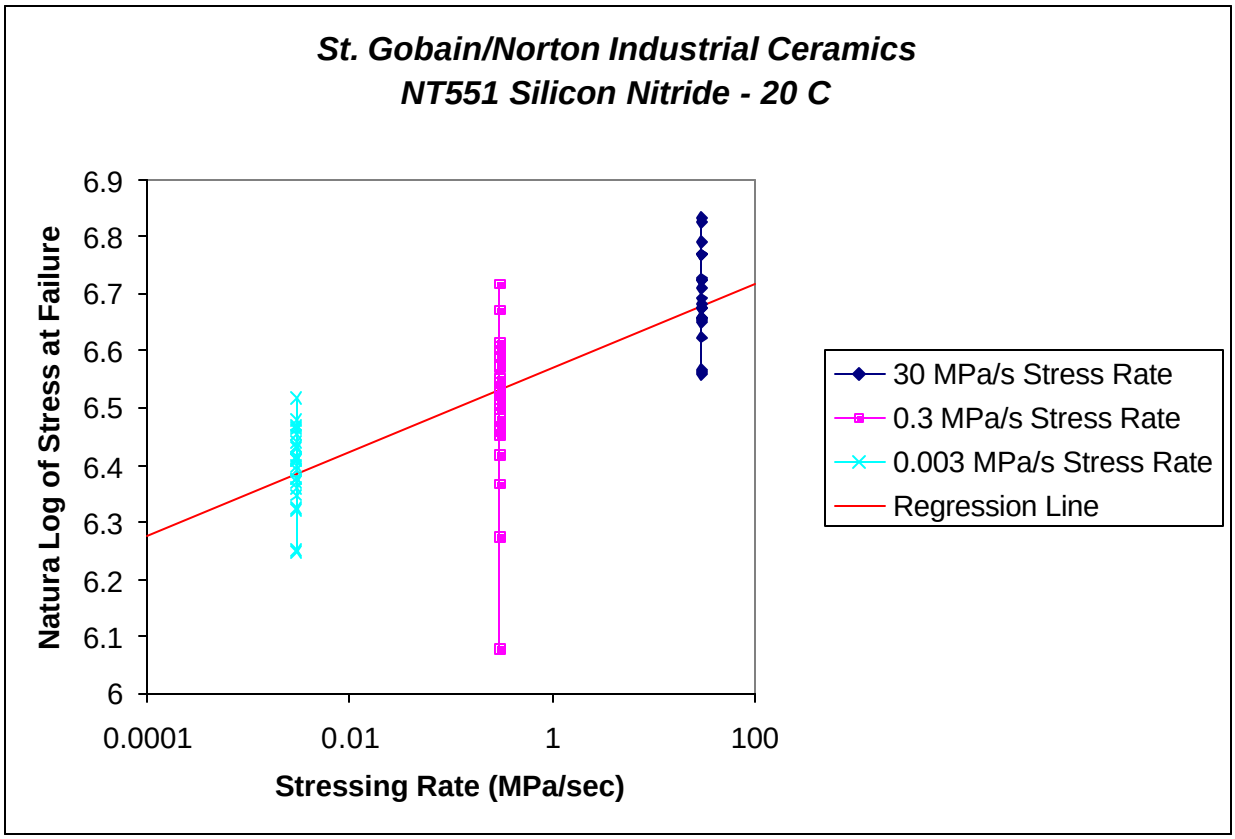

Figure 2 Failure data as a function of stressing rate, and regression line

Pooling Time Dependent Data

If subcritical crack growth is a dominant time dependent failure mechanism in the analysis of ceramic gun barrels, then it would make sense to develop pooling techniques where data from various specimen geometries could be combined into a common data pool in order to estimate improved parameter values. However, up to this point in the project specimen geometries, e.g., C-ring and sectored flex bars, have been developed to interrogate specific flaw populations. Even if fractography could identify common flaw populations between two or more data sets, pooling techniques for censored data are not available for fast fracture data, let alone time dependent data. So the discussion that follows focuses on data sets with a single flaw population.

Conceptually pooling data results in more information available to estimate parameters. Parameter estimates based on a combined data set therefore would yield improved values over the estimates from a single data set. For time dependent failure data (as well as fast fracture data) the key to pooling data this lies in the ability to transform failure data to a common specimen geometry before extracting parameter estimates. The most convenient specimen geometry to convert to is a tensile specimen with a unit gage geometry (volume or area).

Focusing the discussion on data sets with surface defects, then with $kA_T = 1.0$ equations 13 and 35 become

$$\left(\hat{s}\right)^{N+1} = \left({}_1D_A\right)^{N+1}\,\dot{\hat{s}} \tag{36}$$

and

$$B_A = \frac{\left({}_1D_A\right)^{N_A+1}}{\left\{\ln\left[\frac{1}{1-P_f}\right]\right\}^{\frac{N_A-2}{m_A}}\left(s_{0A}\right)^{N_A-2}\left(N_A+1\right)} \tag{37}$$

For an arbitrary test specimen with a surface defect population

$$\left(\hat{s}\right)^{N+1} = \left(D_A\right)^{N+1}\,\dot{\hat{s}} \tag{38}$$

and

$$B_A = \frac{\left(D_A\right)^{N_A+1}}{\left\{\left(\frac{1}{kA_T}\right)\ln\left[\frac{1}{1-P_f}\right]\right\}^{\frac{N_A-2}{m_V}}\left(s_{0V}\right)^{N_A-2}\left(N_A+1\right)} \tag{39}$$

Assuming the same flaw population is interrogated using either the simple tensile specimen with a unit gage surface or an arbitrary test specimen, the true value of B_A would be same for both geometries. Thus equations 37 and 39 are equivalent, which leads to the following relationship

$${}_1D_A = D_A\left(kA_T\right)^{\frac{N_A-2}{m_A(N_A+1)}} \tag{40}$$

To convert failure data for an arbitrary test specimen geometry, take the relationship from equation 40 and insert it into equation 38. This yields the following expression for converted stress values at failure

$$\begin{aligned}
\hat{s} &= \left(D_A\right)\left(\dot{\hat{s}}\right)^{\frac{1}{N_A+1}} \\
\hat{s} &= \left[\frac{\left({}_1D_A\right)}{\left(kA_T\right)^{\frac{N_A-2}{m_A(N_A+1)}}}\right]\left(\dot{\hat{s}}\right)^{\frac{1}{N_A+1}} \\
\hat{s}\left(kA_T\right)^{\frac{N_A-2}{m_A(N_A+1)}} &= \left({}_1D_A\right)\left(\dot{\hat{s}}\right)^{\frac{1}{N_A+1}} \\
\hat{s}_{CONV} &= \left({}_1D_A\right)\left(\dot{\hat{s}}\right)^{\frac{1}{N_A+1}}
\end{aligned} \tag{41}$$

This conversion is similar to the conversion that takes place when pooling fast fracture data.

The conversion and subsequent parameter estimation computations are not without their difficulties. Consider that for surface defects

$$\begin{aligned} kA_T &= \int_A \left(\frac{s}{s_{\max}} \right)^{m_2} dA \\ &= \int_A \left(\frac{s}{s_{\max}} \right)^{\frac{N_A m_A}{m_A - 2}} dA \\ &= kA_T\left(N_A, \ldots\right) \end{aligned} \tag{42}$$

and in addition

$$\begin{aligned} \hat{s}_{CONV} &= \hat{s}\left(kA_T\right)^{\frac{N_A - 2}{m_A(N_A+1)}} \\ &= \hat{s}_{CONV}\left(N_A, \ldots\right) \end{aligned} \tag{43}$$

Thus to make the conversion we need to know the parameter estimate for N_A a priori. However, the data is being pooled in order to improve estimates in N_A (as well as B_A). Thus a numerical algorithm must be developed to minimize the sum of the squares of the residuals, residuals that will be defined in terms of $\hat{s}_{CONV}$. Note that the regression equations for D and N available in *ASTM C 1368* will not be applicable to pooled data. New regression estimators are required.

Summary

A methodology has been established to extract the time dependent parameters B and N from failure data obtained using any type of specimen geometry. These two parameters along with fast fracture Weibull parameters are necessary in conducting time dependent reliability analyses using *CARES/Life*. The parameter estimation technique was demonstrated using a data base available in the open literature since time dependent failure data from the gun barrel program was not available when this report was compiled. Note that bootstrapping methods can be implemented through the use of equation 33. Bounds on parameter estimates using bootstrap techniques would be based on known values of the fast fracture Weibull parameters. Care must be taken to faithfully reproduce the same number of failure data at each stressing rate that appears in the experimental data set. Finally, a pooling approach was outlined in the event that time dependent failure data from multiple specimen geometries representing a single flaw population are made available.

References

Andrews, M.J., Wereszczak, A.A., Kirkland, T.P., and Breder, K., "Strength and Fatugue of NT551 Silicon Nitride and NT551 Diesel Exhaust Valves," *ORNLTM-1999/332*, 1999.

ASTM Standard C 1161-94, "Standard Test Method for Flexural Strength of Advanced Ceramics at Ambient Temperature."

ASTM Standard C 1368-00, "Standard Test Method for Determination of Slow Crack Growth Parameters of Advanced Ceramics by Constant Stress-Rate Flexural Testing at Ambient Temperature."